HOKKAIDO UNIVERSITY

Title	Electron Beam Induced Current Characterization of Novel GaAs Quantum Nanostructures Based on Potential Modulation of Two-Dimensional Electron Gas by Schottky In-Plane Gates
Author(s)	Kasai, Seiya; Hashizume, Tamotsu; Hasegawa, Hideki
Citation	Japanese Journal of Applied Physics. Pt. 1, Regular papers, short notes & review papers, 35(12B), 6652-6658 https://doi.org/10.1143/JJAP.35.6652
Issue Date	1996-12
Doc URL	http://hdl.handle.net/2115/33086
Rights	Copyright © 1996 The Japan Society of Applied Physics
Type	article (author version)
File Information	kasai.pdf

Instructions for use

Hokkaido University Collection of Scholarly and Academic Papers : HUSCAP

Electron Beam Induced Current Characterization of Novel GaAs Quantum Nanostructures Based on Potential Modulation of Two-Dimensional Electron Gas by Schottky In-Plane Gates

Seiya KASAI, Tamotsu HASHIZUME and Hideki HASEGAWA

Research Center for Interface Quantum Electronics and Graduate School of Electronics and Information Engineering, Hokkaido University, Sapporo 060, Japan

(Received July 11,1996 accepted for publication September 17, 1996)

The electron beam induced current (EBIC) technique was used for characterization of novel GaAs quantum nanostructures based on potential modulation of two dimensional electron gas (2DEG) by Schottky in-plane gates (IPGs). A simple theory on the EBIC signal from the basic Schottky IPG structure was developed and it was compared to experimental results. Excellent agreement is between theoretical and experimental results was obtained, indicating that the EBIC technique is a powerful means to detect electric field profiles in depletion layers of quantum nanostructures. The EBIC technique was also applied to Schottky IPG-based quantum wires, lateral superlattices and multi-quantum dot chains. The EBIC study revealed that effective potential control and electron confinement can be achieved by suitable design of Schottky IPG electrodes.

KEYWORDS: electron beam induced current (EBIC), Schottky in-plane gate (IPG), quantum nanostructure, quantum wire, multi-dot chain, lateral superlattice, electric field profile

1. Introduction

The key issue concerning realization of next-generation quantum devices including quantum wave devices and single electron devices is fabrication of defect-free quantum nanostructures. A standard practical nanolithography approach to form semiconductor nanostructures is to combine electron beam (EB) lithography and dry etching. However, the disadvantages of this technique are that the sizes of the nanostructures are usually not small enough, the structure boundaries are very rugged on an atomic scale and the processing introduces damage into the nanostructures.

An alternative approach to overcome the above disadvantages of the standard EB technique is to form quantum structures using the split-gate technique. In this technique, quantum structures are formed by modulating the potential of two-dimensional electron gas (2DEG) at the AlGaAs/GaAs heterointerface with planar Schottky split-gate patterns formed by standard EB lithography. Damage is expected to be small since the place which 2DEG locates is far away from the surface. Potential fluctuations on the lithographically defined rugged surface are smoothened by the long range isotropic nature of the Coulomb force. However, the electron confinement obtainable by the split gate structure is extremely weak, and the quantum wire and single electron devices produced by this technique operate only in the mK range.

To overcome this difficulty of the split-gate technique, we proposed novel quantum nanostructure formation based on the potential modulation of 2DEG by Schottky in-plane gate (IPG) devices including quantum wire transistors[1-3] and single electron transistors.[4] In the novel IPG structure, Schottky gates are formed on side edges of 2DEG as shown in Fig. 1(a). Strong lateral electric fields produced by the Schottky IPG push electrons in the

direction parallel to 2DEG in the present structure and realize the strong confinement of electrons necessary for high temperature operation of quantum effect devices. A slightly modified cross structure Fig. 1(b) is obviously possible also and may be more useful in some device applications. This technique can be used for formation of quantum wires, lateral superlattices and single and multi-quantum dots whose sizes are voltage tunable as shown in Figs. 1(c)-1(f).

For successful design and realization of such novel nanostructures utilizing Schottky IPGs, development of a suitable structural characterization technique is obviously desirable, since the depletion layer edges defining the quantum structure boundaries are buried in the structure and are not directly visible by standard scanning electron microscope (SEM) observation.

The purpose of the present paper is to characterize Schottky IPG-based GaAs quantum nanostructures by the electron beam induced current (EBIC) technique. A simple theory on EBIC signals from the basic Schottky/2DEG diode is developed and theoretical results are compared to experimental results. The results of comparison indicate that the EBIC technique is a powerful means to detect electric field profiles in the buried depletion layers. Then, the EBIC technique is applied to various Schottky IPG-based quantum nanostructures, including quantum wires, lateral superlattices and multi-quantum-dot chains, and it is directly confirmed that the successful formation of intended structures.

2. A Theory for EBIC Characterization of Schottky IPG Structures

2.1 Basic equations for EBIC analysis

In the EBIC measurement, the charge carriers generated by an electron beam are collected and detected as current in an external circuit. In particular, when a fine electron beam is irradiated at a position x, in the depletion layer with a width W_{dep}, electron-hole pairs generated by irradiation of the electron beam are separated by the strong electric field in the depletion region, as shown in Fig. 2. These electrons and holes then drift in opposite directions and produce a current in the external circuit, if all of them do not recombine in the depletion region. According to a previous work,[5] current $J(x)$ can be generally expressed by the following equation.

, (1)

where G is the electron-hole pair generation rate, q is electronic charge, I_B is the electron beam current, E_B is the electron beam energy, $E_{e\text{-}h}$ is the energy required for electron-hole pair generation, f is the surface reflectivity for the electron beam and · is the collection efficiency. The value of the collection efficiency · is determined by the carrier dynamics in the depletion region. For example, for a depletion layer having a uniform field E, a carrier mobility μ and a SRH recombination lifetime τ, · is given by[5]

, (2)

where SRH recombination in the depletion layer is negligible, γÇ1 and eq. (2) gives ·=1. Thus, $J(x)=G$, being independent of the field E. On the other hand, when SRH recombination is frequent, $\cdot=\gamma^{-1}=\mu\tau E/W_{dep}$ and the current becomes proportional to E. In devices based on single crystalline Si, normally γÇ1, and one cannot obtain information concerning E from the EBIC signal. Thus, the EBIC technique has been utilized for determination of diffusion length L and surface recombination velocity S.

In the case of GaAs, SRH recombination is similarly negligible. However, extremely strong radiative recombination takes place particularly due to its direct energy gap, producing cathode luminescence, as schematically shown in Fig. 2. In this case, it is easy to show that $J(x)$ is given by the following equation.

, (3)

where τ_n is the effective radiative recombination time for cathode luminescence. This equation shows that the EBIC signal directly reflects the electric field in the structure if the generated equilibrium carrier density n_0 is the same everywhere. Thus, if one uses an extremely high-resolution SEM system where the radius of the beam can be ignored, the signal gives potential distribution directly.

In practice, however, it is known that the area where electron-hole pairs are produced has a finite extension even if the radius of the electron beam is sufficiently small. This is due to the fact that the high energy electrons move within the material during electron-hole pair generation. The simplest way to take this effect account into is to make a superposition of eq. (3). Then,

, (4)

where R_X (x) is the distribution function of generated carriers. Assuming that this distribution is Gaussian, the current is given by the next equation.

, (5)

where R_e is the electron range. It is known empirically that the value of R_e depends on the energy of the electron beam, E_B,[5] as

(cm) , (6)

where ρ is the density of the sample (g/cm^3).

2.2 EBIC signal from basic Schottky IPG/2DEG diode

For theoretical evaluation of EBIC signals using eq. (5), one requires knowledge of the field distribution. Since a rigorous analysis of the complicated device structure in Fig. 1 requires detailed three-dimensional potential analysis, only the basic Schottky IPG/2DEG diode is treated quantitatively for the purpose of comparison with the experimental results. A simple model for the Schottky IPG structure used here is shown in Fig. 2(a), where a perpendicular IPG is formed at the edge of 2DEG. It is also assumed that the carrier supply layer to 2DEG is a δ- doped one with a zero spacer thickness for simplicity. Then the longitudinal electric field distribution $E(x)$ along the x-axis and the depletion width $W_{dep}(V)$ of the basic Schottky IPG diode can be approximately described analytically by the eqs. (7a) and (7b), respectively.[6]

(7a)

, (7b)

where n_s is the sheet carrier concentration of 2DEG, V is the gate voltage and V_{bi} is the

built-in potential of the Schottky barrier. These equations are to be compared with the following equations for a conventional planar Schottky contact on the three-dimensional electron gas (3DEG) shown in Fig. 3(b).

(8a)

and

, (8b)

where N is the ionized impurity concentration. Some examples of the calculated field distributions are shown for both structures in Fig. 3(c) for the purpose of comparison. It should be noted that the field strength is significantly large for the Schottky IPG/2DEG structure with the same value of (V_{bi}V).

Figure 4(a) shows the calculated normalized EBIC signals using eqs. (5), (6), (7a) and (7b) for the Schottky IPG/2DEG diode for different values of E_B. ρ =4.71 g/cm^3 was used for GaAs. For comparison, calculated signals for a conventional Schottky contact are shown in Fig. 4(b). It is observed that use of higher acceleration voltages of the electron beam quickly broadens the EBIC signal.

Since the field profile is thus quickly broadened and distorted by the penetration effect of the electron beam, it is difficult to directly determine the depletion layer edge from the EBIC signal profile. Diffusion effects of carriers outside the depletion layer, which are ignored in the present simplified analysis may produce a long tail in the EBIC signal profile and may cause further difficulty in determining the edge position. This difficulty may be alleviated by theoretically relating the effective width of the EBIC signal to the depletion width.

Figure 5 shows an example of the calculated relationship between W_{dep}, and the full

width at half maximum (FWHM), *ÆW*, of the EBIC signal for the IPG Schottky contact. It is seen that *ÆW* increases almost linearly with the increase of W_{dep}. Using this relationship, the value of W_{dep} of the Schottky IPG structure can be estimated from the measured value of *ÆW*. For this purpose, the value of E_B should be kept reasonably small since the slope of the signal curve for a higher EB energy is small and less sensitive to variation of W_{dep}.

3. Experimental EBIC Characterization of Basic Schottky IPG Structure

3.1. Sample structure and EBIC measurement

The experimental setup and the sample structure used for EBIC characterization of the basic Schottky IPG structure is shown in Fig. 6. The sample was fabricated as follows. First, an $Al_{0.3}Ga_{0.7}As$/GaAs double heterostructure wafer with a GaAs well width of 20 nm was grown by standard MBE growth at substrate temperature of 600¡C. The 2DEG was located 60 nm below the surface. δ- doping by Si was performed 10 nm the above 2DEG. Then, the edge of the 2DEG was revealed by wet chemical etching down to 500 nm. Subsequently, Schottky IPG electrodes were defined by photolithography or EB lithography and formed by Pt plating using an in-situ electrochemical process.[7)]

For EBIC measurement, Hitachi S4100 SEM equipment with a spatial resolution of 10 nm was used. The beam voltage was varied from 2 to 15 keV. The EBIC measurement system which was attached to a SEM was equipped with a bias-voltage application circuit to measure the bias dependence of the EBIC signal. The electron beam was scanned on the top surface or on the cross section of the samples, as shown in Fig. 6.

3.2 Observed EBIC signals and comparison with theory

The examples of the EBIC line scan signal from the Pt/2DEG Schottky diode sample are shown for different bias voltages in Figs .7(a) and 7(b). The value of E_B was 5 keV for Fig. 7(a), and 10 keV for Fig. 7(b). By comparing Fig. 7 with Fig. 4(b), it is seen that experimentally observed signal shapes, their bias-voltage dependence and their beam-energy dependence qualitatively agree with those predicted by the theoretical calculation. However, quantitatively speaking, it is notable that the tail of the observed EBIC signal is more prolonged and maintains a higher level than the calculated one. This seems to be due to diffusion current components which are totally ignored in the present analysis.

For further quantitative comparison between theoretical and experimental results, experimentally observed bias dependences of *ÆW* of the EBIC signal are plotted in Fig. 8(a) for various values of E_B. The theoretical curves n_s=5x10^{11} cm^{-2} and V_{bi} =0.7 eV confirmed by the Hall measurement and capacitance-voltage measurement,[8] are also shown in Fig. 8(a). It is seen that the theoretical curves agree excellently with the experimental results for each EB energy condition in spite of the aforementioned discrepancy in the tail portion of the EBIC signal. This indicates that the additional diffusion current components are not large enough to alter the main feature of the EBIC signal reflecting drift components.

In Fig. 8(b), the values estimated from the relationship between W_{dep} and *ÆW* in Fig. 5 are directly compared with the theoretical curves based on eq. (7b). Again, excellent agreement between theory and experiment is obtained, resulting overall consistency. Therefore, the novel EBIC method is extremely useful for not only qualitative, but also

quantitative characterization of the electric field and potential distributions controlled by the Schottky IPGs.

4. EBIC Characterization of Various Quantum Nanostructures Based on Schottky IPGs

4.1 Quantum wires

With the present Schottky IPG approach, voltage-tunable quantum wires can be formed using the electrode arrangement shown in Fig. 1(c). In the present study, a wire having a cross section as shown in Fig. 1(a) was fabricated and studied by EBIC. The structure of the sample is shown in Fig. 9(a). The sample was prepared by applying EB lithography and wet chemical etching to an AlGaAs/GaAs QW wafer. A plan view SEM micrograph of the sample is shown in Fig. 9(b).

Figure 9(c) shows a line scan EBIC signal taken on the SEM plan view of the sample at zero bias. Two fine peaks were clearly observed at the edge of the wire, showing the existence of depletion layers in the channel. This clearly demonstrates that in this case the EBIC technique allows non-destructive characterization of buried depletion boundaries.

As reported elsewhere,[9] this quantum wire exhibited the existence of the first plateau of quantized conductance in units of $2e^2/h$ up to 100 K in spite of its large waveguide length of more than 1,000 nm. This value is much higher than the value of 53 K obtained with a AlGaAs/GaAs split-gate point contact formed using much smaller dimensions, and shows that a very strong confinement potential can be achieved by the

present Schottky IPG structure.

4.2 Lateral superlattices and multi-dot structures

As shown in Fig. 1(e) and 1(f), lateral superlattices and multi-dot chains can be easily realized by suitable Schottky IPG patterns to a 2DEG bar. Potential modulation can be achieved by gate bias, use of different Schottky barrier heights (SBHs) or periodic insertion of air gaps. To test the feasibility of these novel approaches, samples shown in Fig. 10 were fabricated and characterized by the EBIC technique. The samples had the cross section shown in Fig. 1(b).

Figure 10(a) shows the fabricated lateral superlattice structure, utilizing a periodic array of Schottky IPGs with different SBHs, ϕ_{B1} and ϕ_{B2}. Due to the Fermi level pinning on GaAs and AlGaAs, realization of different SBHs achieved by using metals with different work functions is almost impossible. Here, periodic insertion of an As doped silicon interface control layer (Si ICL) was employed as shown in Fig. 10 where doping-dipole formed in the As-doped Si ICL reduces the SBH.[10)]

SEM and EBIC images taken of the cross section of the sample along the center line *x*-*x*′ in Fig. 10(a) are shown in Figs. 11(a) and 11(b). Figure 11(b) clearly and directly demonstrates that periodic variation of SBH is indeed realized by the insertion of Si ICL stripes. The result of EBIC line scans along lines *a* and *b* in Fig. 10(b) is shown in Fig. 11(c). The difference in SBH can be seen more clearly here. A further quantitative analysis showed that SBH without Si ICL was 0.8 eV and that with Si ICL was 0.6 eV, which was consistent with the results of separate C-V measurements on Schottky diodes with larger

dimensions. Thus, the EBIC allows direct analysis of buried field profiles of nanostructures. As reported elsewhere,[11] this type of lateral superlattice showed clear transconductance and drain conductance oscillations at low temperature.

Figure 10(c) shows yet another periodic structure utilizing periodic insertion of air gaps. This structure can be operated as lateral superlattices and multi-dot chains, depending on the applied gate voltage. This structure was also fabricated by EB lithography, etching and deposition of the Cr/Au Schottky metal, and was characterized by the SEM/EBIC technique.

The cross-sectional SEM image and EBIC line scan of the portion having a Cr/Au Schottky IPG is shown in Fig. 12(a) and (b). The top width of the 2DEG bar was 1 μm and the height of the mesa pattern was 200 nm. The 2DEG was located 60 nm from the top M-S interface. The line scan of the EBIC image near the heterointerface under zero bias is shown in Fig. 12(b). From the value of ΔW of the EBIC edge peaks at E_B =5 keV of about 250~300 nm, the depletion width was estimated to be about 70~80 nm using the present analysis. This value is reasonable, since the calculated value using eq. (6a) is 60 nm with n_S=1.8x10^{12} cm^{-2} according to Hall measurement.

Figure 12(c) shows the plan view SEM image of the fabricated structure having 38 stripes. The Schottky IPG width was 40 nm and the interval of the IPG gate was 160 nm, corresponding to a gate periodicity of 200 nm.

As will be reported elsewhere,[12] this device has shown clear Coulomb oscillation characteristics near pinch-off of up to 5.4 K, in spite of a channel 1,300 nm, indicating successful multi-dot formation. The maximum temperature for observation of Coulomb blockade oscillation is much higher than that for usual split-gate SET devices, which show oscillation of up to a few hundred mK. This result confirms that very effective confinement

of electrons can be achieved by the Schottky IPG structure.

5. Conclusion

Characterization of the depletion field profiles within the Schottky IPG-based GaAs quantum nanostructures by the EBIC technique was attempted. Main conclusions are as follows.

1) The simple theory on the EBIC signal from the basic Schottky IPG/2DEG developed here can explain the experimental results very well.

2) By taking the range of the electron beam into account a direct, non-destructive and quantitative characterization of field profiles, depletion widths and Schottky barrier heights of the buried depletion layer becomes possible.

3) The results of applications of the EBIC technique to wires, lateral superlattices and multi-dot structures reveal the effectiveness of the Schottky IPG controls of 2DEG for realization of defect-free compound semiconductor quantum nanostructures.

References

1) H. Hasegawa, T. Hashizume, H. Okada and K. Jinushi: J. Vac. Sci. & Technol. B **13** (1995) 1744.

2) H. Okada, T. Hashizume and H. Hasegawa: Jpn. J. Appl. Phys. **34** (1995) 6971.

3) H. Okada, K. Jinushi, N. -J. Wu, T. Hashizume and H. Hasegawa: Jpn. J. Appl. Phys. **34** (1995) 1315.

4) K. Jinushi, H. Okada, T. Hashizume and H. Hasegawa: Jpn. J. Appl. Phys. **35** (1996) 397.

5) H. J. Leamy: J. Appl. Phys. **53** (1982) R51.

6) B. Gelmont, M. Shur and C. Moglestue: IEEE Trans. Electron Device **39** (1992) 1219.

7) T. Hashizume, G. Schweeger, N. -J. Wu and H. Hasegawa: J. Vac. Sci. & Technol. B **12** (1994) 2660.

8) T. Hashizume, H. Okada, N. -J. Wu and H. Hasegawa: Jpn. J. Appl. Phys. **34** (1995) 1149.

9) T. Hashizume, H. Okada and H. Hasegawa: *Tech. Dig. of 3rd Int. Symp. New Phenomena in Mesoscopic Structure*, Maui, December, 1995, Q16.

10) K. Koyanagi, S. Kasai and H. Hasegawa: Jpn. J. Appl. Phys. **32** (1993) 502.

11) S. Kasai and H. Hasegawa: Jpn. J. Appl. Phys. **35** (1996) 1340.

12) S. Kasai, K. Jinushi, H. Okada, H. Tomozawa, T. Hashizume and H. Hasegawa: *Ext. Abstr. 1996 Int. Conf. Solid State Devices and Materials* (Business Center for Academic Societies, Japan, Tokyo, 1996) p.443.

Figure caption

Fig.1. Novel Schottky IPG structures.

Fig.2. Basic idea of electron beam induced current.

Fig.3.Simple model for (a) Schottky IPG to 2DEG and (b) planar Schottky contact on 3DEG.

Fig.4. Calculated EBIC signals for (a) Schottky IPG and (b) planar Schottky contacts.

Fig.5. Calculated FWHM *ÆW* of EBIC signal as a function of depletion layer width W_{dep}.

Fig.6. EBIC measurement system.

Fig.7. Examples of line scan EBIC signals from Pt/2DEG Schottky IPG diode.

Fig.8. (a) FWHM of EBIC signal and (b) estimated depletion layer width as a function of applied voltage.

Fig.9. (a) Device structure, (b) plan view SEM image and (c) line scan EBIC signal of the Schottky IPG quantum wire.

Fig.10. (a) Lateral superlattice structure utilizing a periodic arrays of Schottky IPGs with different SBH, (b) cross section of the structure and (c) lateral superlattice with periodic IPGs and air-gaps.

Fig.11. Cross-sectional (a) SEM, (b) EBIC image of the lateral superlattice structure and (c) line scan EBIC signals.

Fig.12. (a) Cross sectional SEM image, (b) line scan EBIC signal of the Schottky IPG structure and (c) plan view SEM image of the multi-dot structure by Schottky IPGs.

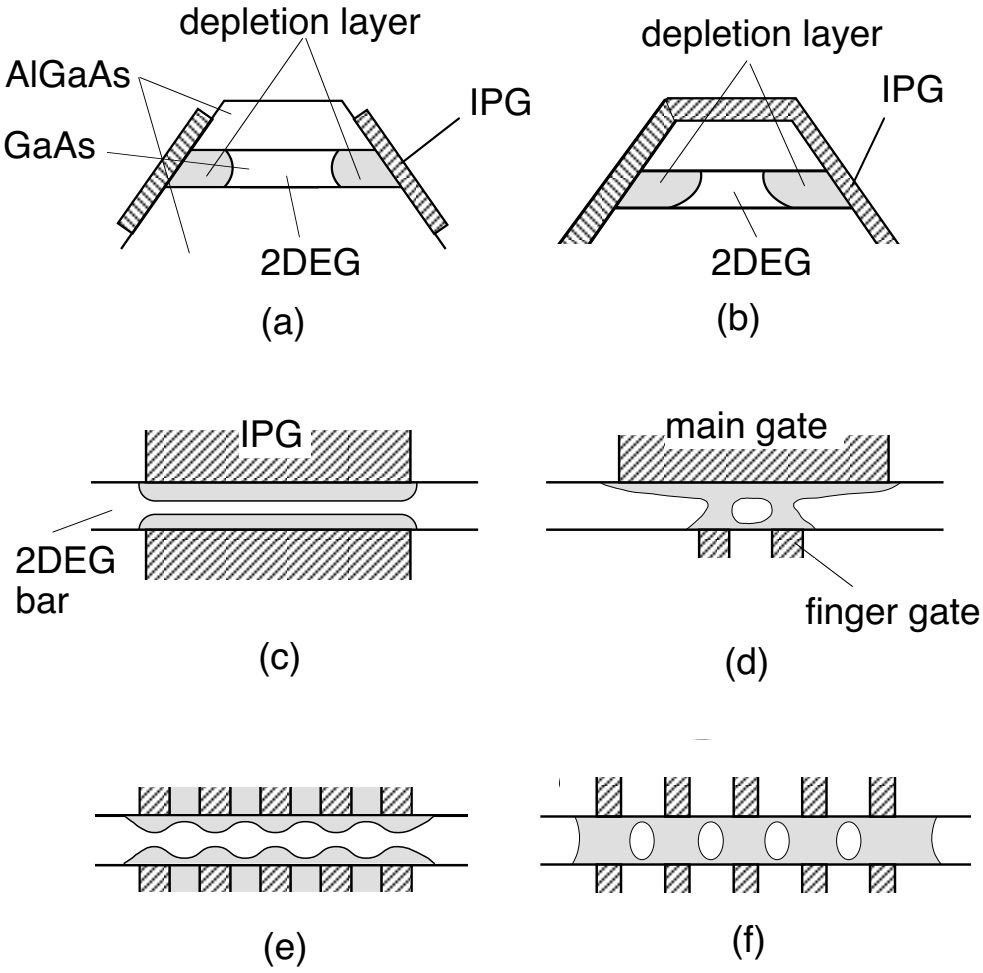

Fig.1
S.Kasai et al.

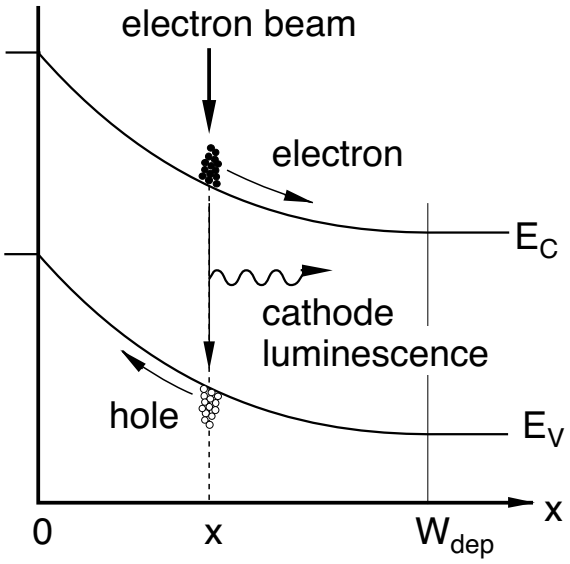

Fig.2
S.Kasai et al.

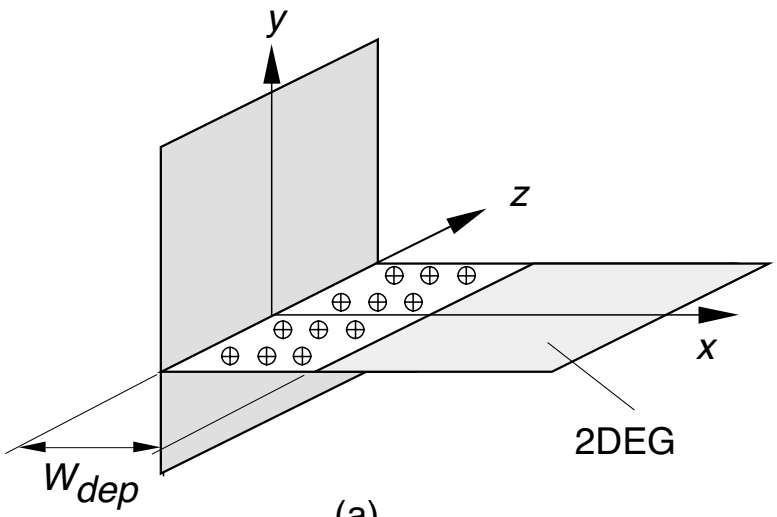

(a)

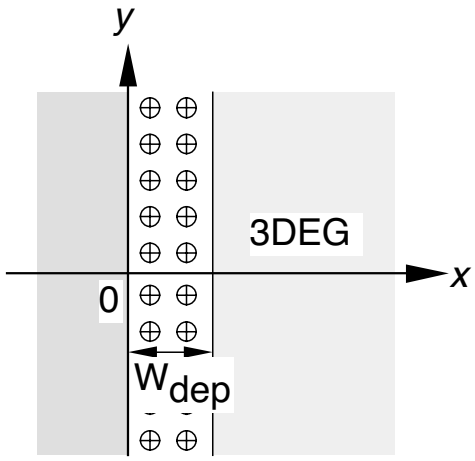

(b)

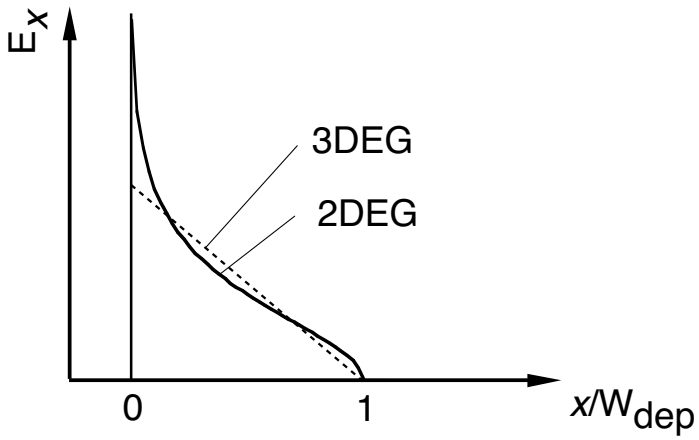

(c)

Fig.3
S.Kasai et al.

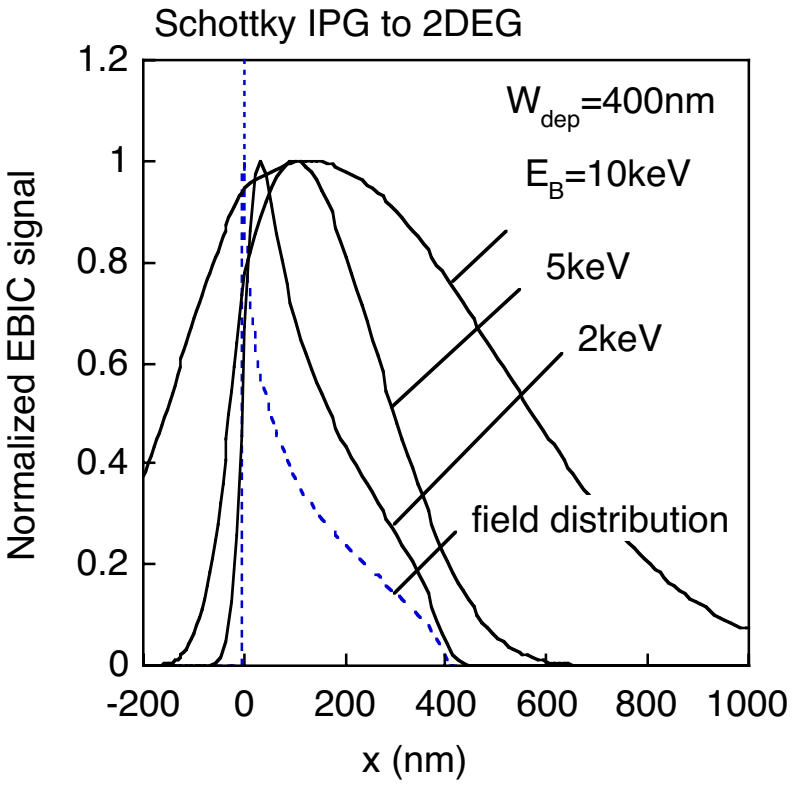

(a)

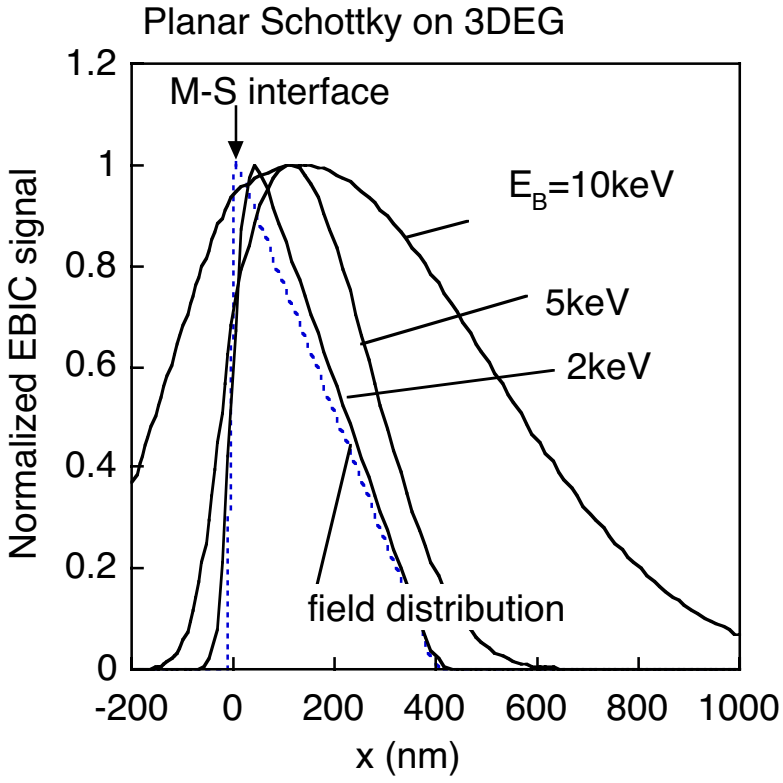

(b)

Fig.4 S.Kasai et al.

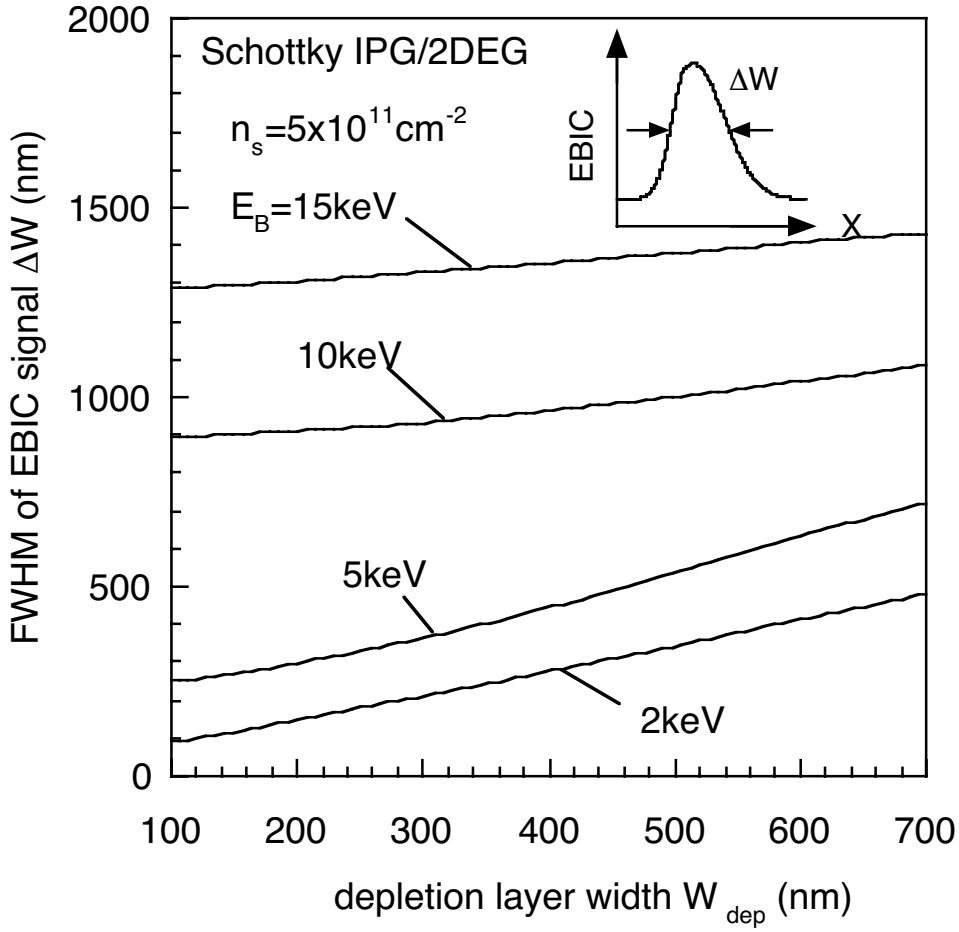

Fig.5 S.Kasai et al.

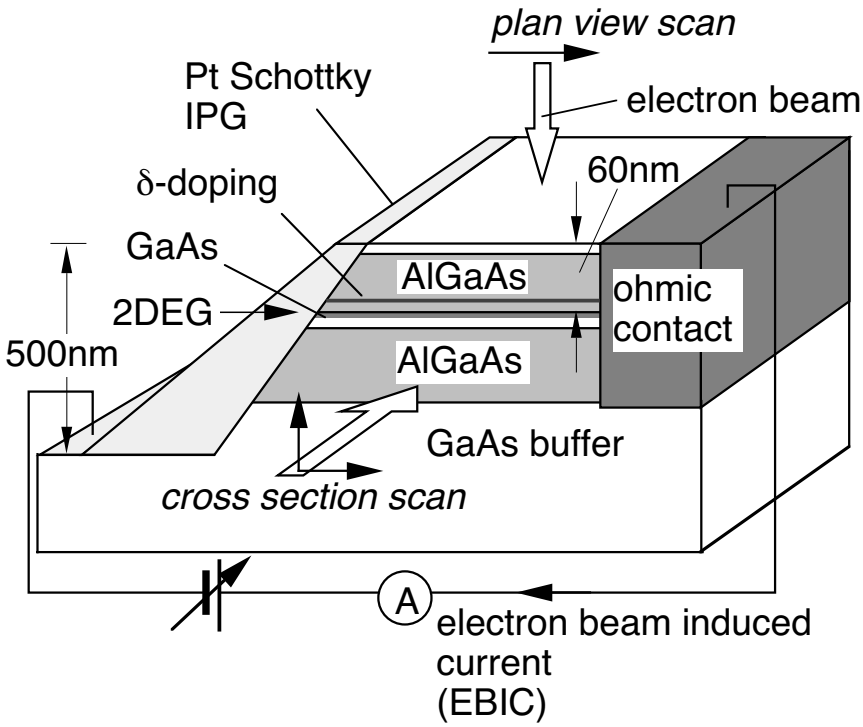

Fig.6
S.Kasai et al.

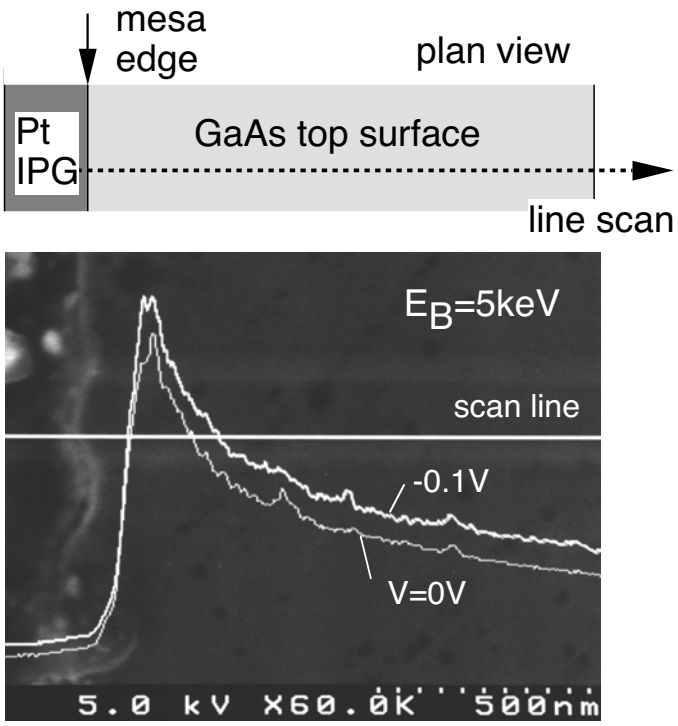

(a)

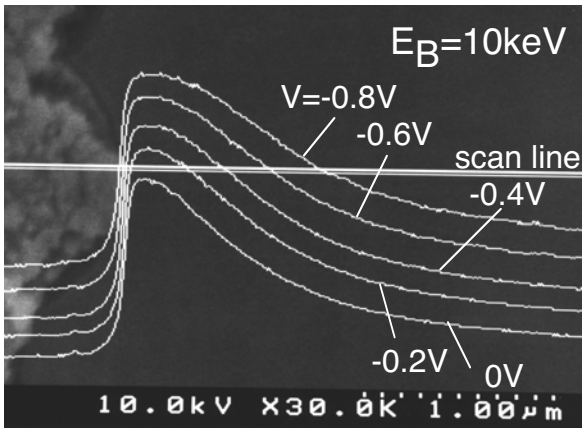

(b)

Fig.7
S.Kasai et al.

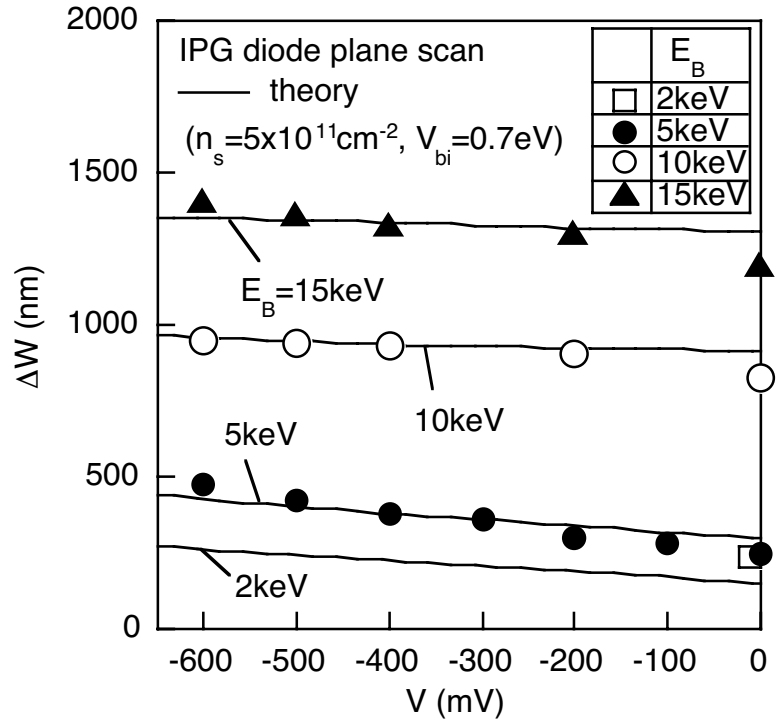

(a)

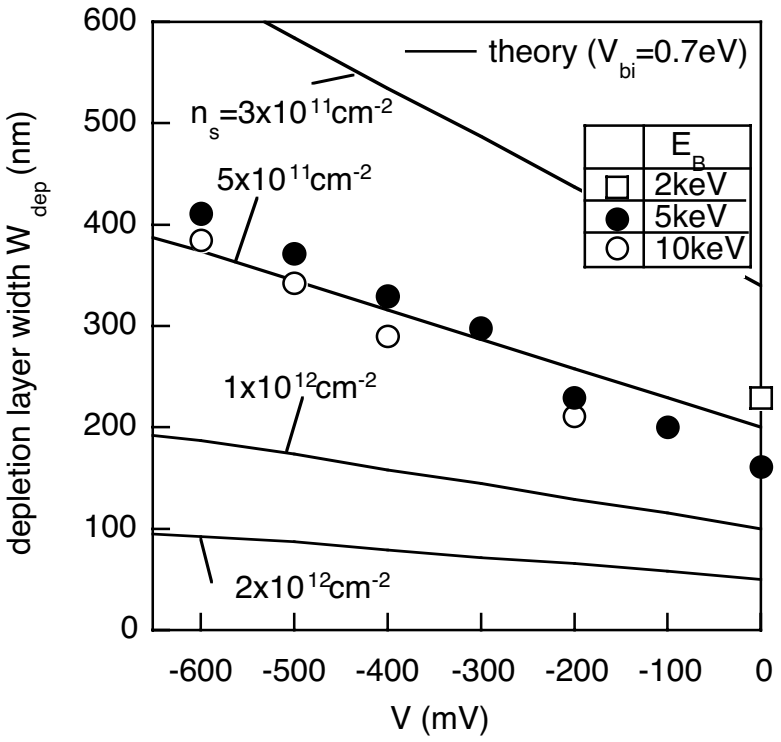

(b)

Fig.8 S.Kasai et al.

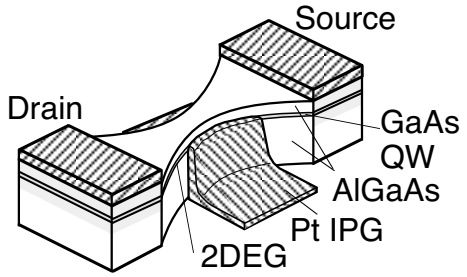

(a)

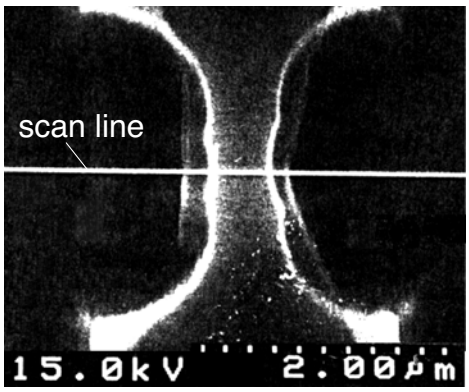

(b)

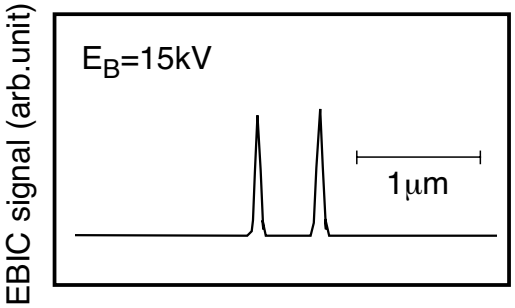

(c)

Fig.9
S.Kasai et al.

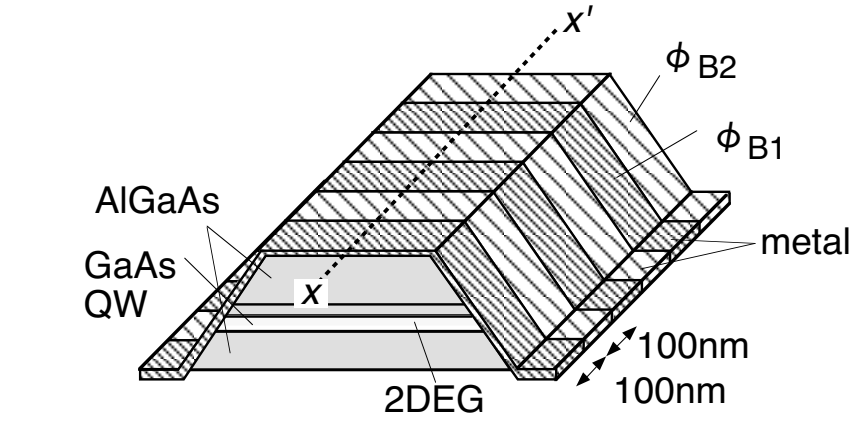

(a)

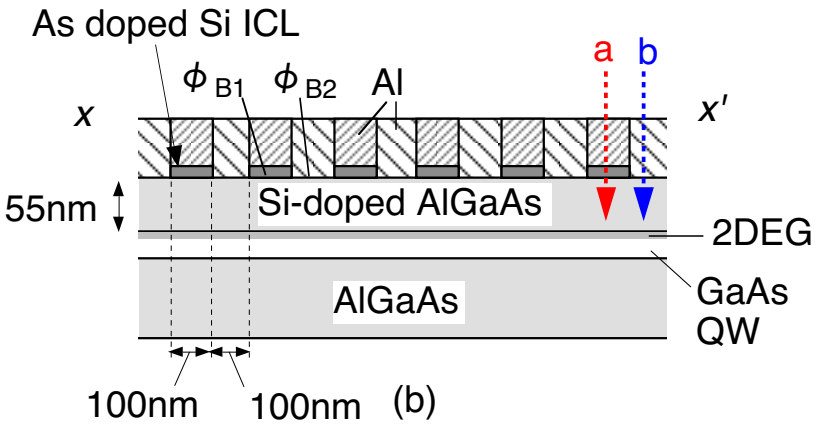

(b)

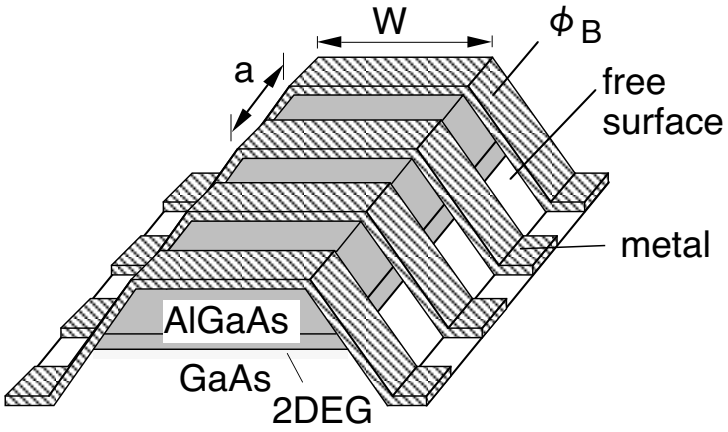

(c)

Fig.10
S.Kasai et al.

SEM image

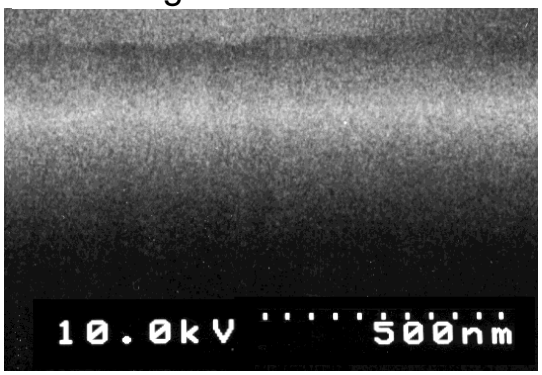

Al

GaAs/
AlGaAs

(a)

EBIC image

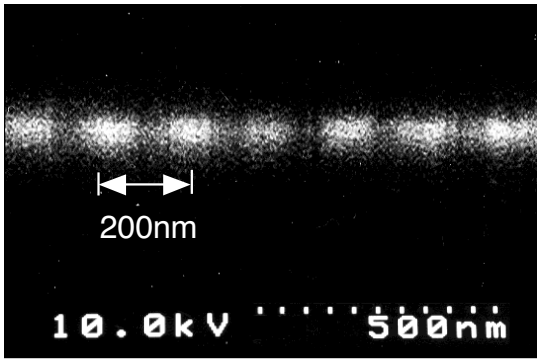

Al

GaAs/
AlGaAs

(b)

EBIC line scan (E_B=10kV)

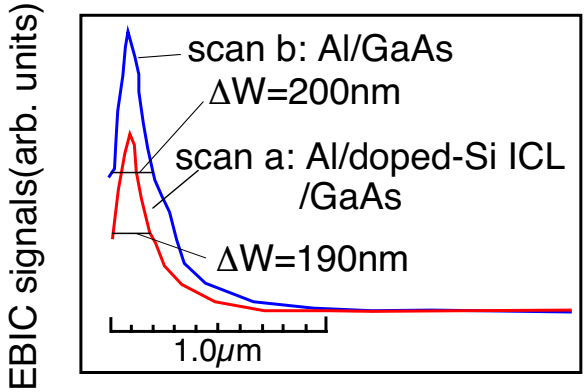

(c)

Fig.11
S.Kasai et al.

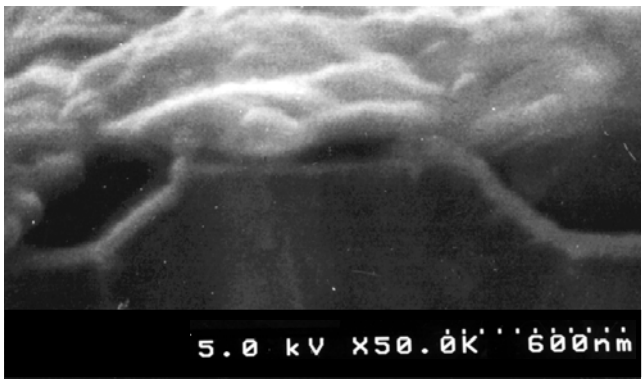

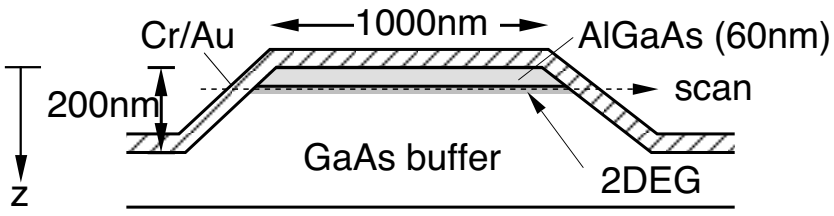

(a)

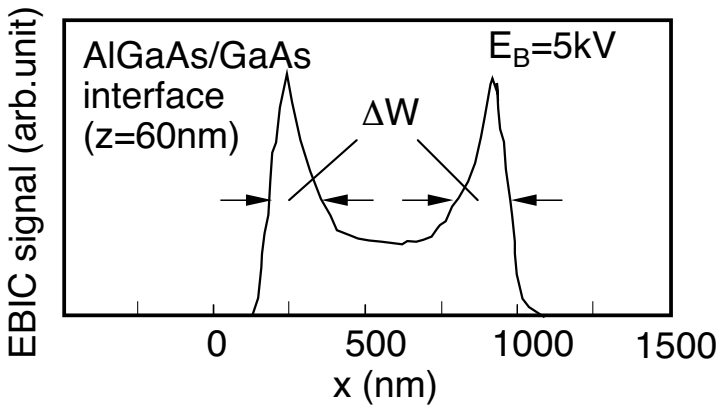

(b)

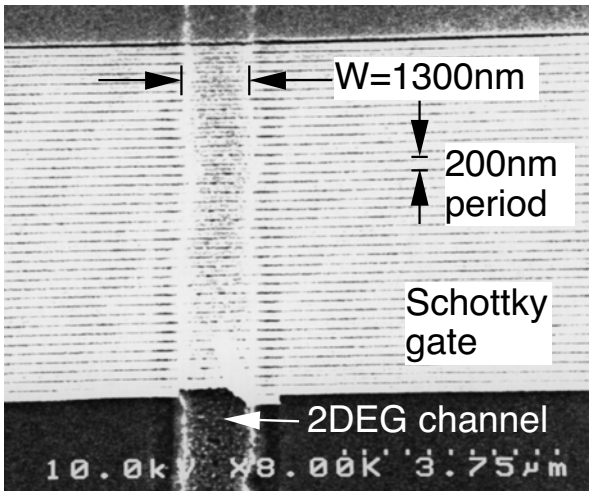

(c)

Fig.12
S.Kasai et al.